J. Fluid Mech. (1972), *vol.* 53, *part* 2, *pp.* 287–303
Printed in Great Britain

Jets induced by oscillatory motion

By B. J. DAVIDSON AND N. RILEY
School of Mathematics and Physics, University of East Anglia, Norwich

(Received 17 September 1971)

The flow induced by a cylinder performing transverse periodic oscillations in a fluid which is otherwise at rest is investigated. The motion of the cylinder is not necessarily harmonic. Attention is focused upon the induced steady streaming. In particular, the jet-like flow which arises when the streaming Reynolds number is large is studied. The theoretical results obtained are applied to a class of elliptic cylinders, and a simple experimental investigation is carried out which substantiates the main theoretical conclusions.

1. Introduction

In this paper we are concerned with the flow induced by a cylinder which performs periodic transverse vibrations in a viscous fluid which is otherwise at rest. We suppose that the cylinder speed along its axis of oscillation is given by $U_\infty f(t')$, where it is convenient to define U_∞ in such a way that $\max |f(t')| = 1$. The speed is taken to be periodic with period $2\pi/\omega$ so that $f(t' + 2\pi/\omega) = f(t')$, where t' represents the time. In the theoretical development of § 2 we find it convenient to represent $f(t')$ as

$$\left.\begin{aligned} f(t') &= \sum_{n=1}^{\infty} \{a_n \cos \omega n t' + b_n \sin \omega n t'\}, \\ &= \sum_{n=1}^{\infty} \alpha_n \cos(\omega n t' + \beta_n), \quad \text{say.} \end{aligned}\right\} \tag{1}$$

With U_∞ as a typical velocity, ω^{-1} as a typical time and ν the kinematic viscosity of the fluid, there are three length scales associated with this problem. These are $a = U_\infty/\omega$, which is a measure of the amplitude of the oscillation, $\delta = (\nu/\omega)^{\frac{1}{2}}$, which represents the thickness of the Stokes layer present at the cylinder surface, and a geometrical length d, which is representative of the dimensions of the cylinder. From these three length scales we can construct two independent dimensionless parameters which characterize the motion. These we choose as

$$\left.\begin{aligned} \epsilon &= a/d = U_\infty/\omega d, \\ R_s &= a^2/\delta^2 = U_\infty^2/\omega\nu, \end{aligned}\right\} \tag{2}$$

and in our theoretical development we suppose that $\epsilon \ll 1$ with $R_s = O(1)$ and assume that our results are asymptotically valid as $\epsilon \to 0$ with $\lim R_s < \infty$. For small amplitude vibrations the choice of ϵ as a perturbation parameter is an obvious one; the choice of R_s as the second independent parameter is less obvious.

However, for the case of a cylinder vibrating in simple harmonic motion, Stuart (1963) has argued that R_s is in fact the Reynolds number associated with the steady streaming which persists outside the Stokes layer, and this point has been further pursued by Riley (1967). Since R_s plays the same role in the present investigation, the central theme of which is the induced steady streaming, it emerges as a natural parameter, along with ϵ, to characterize the flow.

With U_∞, ω^{-1} and d as a typical velocity, time and length respectively, the equation satisfied by the dimensionless stream function ψ is

$$\left[\frac{\partial}{\partial t}(\nabla^2\psi) - \epsilon\frac{\partial(\psi, \nabla^2\psi)}{\partial(x, y)} = \frac{\epsilon^2}{R_s}\nabla^4\psi, \right. \tag{3}$$

where ∇^2 is the two-dimensional Laplace operator.

If the co-ordinate system $\mathbf{x} = (x, y)$ is supposed fixed in the cylinder then the boundary conditions for (3) are

$$\left.\begin{aligned} &\mathbf{v} = 0 \text{ on the cylinder,} \\ &\psi \sim y\sum_{n=1}^{\infty} \alpha_n e^{i(nt+\beta_n)} \quad \text{as} \quad |\mathbf{x}| \to \infty, \end{aligned}\right\} \tag{4}$$

where the x axis has been chosen to be parallel to the direction of oscillation and the real part of any complex quantity is to be understood. All the variables in (3) and (4) are dimensionless.

The fact that a steady streaming may be induced by a periodic motion of the cylinder is most readily appreciated from (3) by considering a single component of (1). Thus, to first order, if $\psi \sim \cos(nt+\beta_n)$ then the $O(\epsilon)$ equations can contain forcing terms which contribute a steady part in addition to the expected higher harmonics. The method of solution of (3) for $\epsilon \ll 1$, developed in § 2, follows closely that given by Riley (1967) for a cylinder performing a simple harmonic motion and in turn reflects the work of Longuet-Higgins (1953). Complementary series solutions in powers of ϵ are assumed in both an outer region, distance $O(1)$ from the cylinder, and an inner Stokes layer of thickness $O(\epsilon/R_s^{\frac{1}{2}})$. To each order of ϵ these series solutions must match asymptotically. Clearly, for those parts of the theory where only linear equations are involved, the results for the general periodic motion (1) of the cylinder may be inferred from a suitable superposition of the earlier results for a purely sinusoidal motion. However, as we have demonstrated above, the steady streaming phenomenon is a result of interactions associated with the nonlinear terms in (3). Nevertheless, it can be shown that the principal results pertaining to the steady streaming are closely related to those which are obtained when the motion of the cylinder is represented by only a single term of (1). Thus in the outer region the streaming is governed by the full Navier–Stokes equation with R_s as the Reynolds number. The streaming is driven indirectly from that within the Stokes layer which is itself a direct consequence of the action of the Reynolds stresses; these stresses, for the purely sinusoidal case, are not present in the outer region.

For the case $R_s \gg 1$, but with $\epsilon R_s^{\frac{1}{2}} \ll 1$ in accordance with our assumed limit process,† the outer streaming itself assumes a boundary-layer character, of

† Since in the double-limit process $\epsilon \to 0$, $R_s \to \infty$, the limit $\epsilon \to 0$ is carried out first.

thickness $O(R_s^{-\frac{1}{2}})$. This outer boundary layer has been the subject of studies by Riley (1965) and Stuart (1966) for the case of a cylinder vibrating as a pure sinusoid. These authors conclude that, for a symmetrical body say, the outer boundary layers develop from stagnation points of attachment leading to an inevitable 'collison' at the axis of oscillation, along which the fluid then moves out in a jet-like manner. In this paper, for $R_s \gg 1$, we first show that for a cylinder whose velocity is described by (1), the characteristics of the motion in the outer boundary layer may be immediately inferred from those in the case of a cylinder performing purely sinusoidal oscillations. We then extend, in § 3, the work of Riley and Stuart by performing a complete numerical integration of the boundary-layer equations for a class of elliptic cylinders. In this way we are able to calculate the strength of the jet which emerges along the axis of oscillation. In § 4 we describe a simple experiment which has been performed to supplement the theoretical work. In the experiments the cylinder vibrates transversely in a tank of water. The jet, to which we have referred above, is visualized by placing a thin wire perpendicular to the axis of vibration and intermittently passing an electric current through the wire. Lines of hydrogen bubbles are released and clearly show the jet-like structure of the flow. From these experiments, quantitative measurements have been made of the momentum flux in the jet, and the jet profiles have been compared with those predicted by Bickley (1937). The agreement between theory and experiment is, we believe, very encouraging.

2. Development of the theory

With $\epsilon \ll 1$ and $R_s = O(1)$ we seek a solution of (3), subject to (4), in the form

$$\psi = \sum_{m=0} \epsilon^m \psi_m(\mathbf{x}, t, R_s), \tag{5}$$

where, from our discussion in § 1, we further write

$$\psi_1 = \psi_1^{(u)}(\mathbf{x}, t, R_s) + \psi_1^{(s)}(\mathbf{x}, R_s) \tag{6}$$

in anticipation of the assumed steady streaming of $O(\epsilon)$. Substituting (5) into (3), we find that ψ_0 satisfies

$$\left.\begin{aligned} \partial(\nabla^2\psi_0)/\partial t &= 0, \\ \psi_0 &= 0 \quad \text{on} \quad \tilde{y} = 0, \\ \psi_0 &\sim y \sum_{n=1}^{\infty} \alpha_n e^{i(nt+\beta_n)} \quad \text{as} \quad |\mathbf{x}| \to \infty, \end{aligned}\right\} \tag{7}$$

in which the no-slip condition, which cannot be satisfied by ψ_0, has been relaxed. In (7), and in what follows, it proves convenient in the neighbourhood of the body to work not with co-ordinates (x, y) but with orthogonal co-ordinates $\tilde{\mathbf{x}} = (\tilde{x}, \tilde{y})$, where $\tilde{y}$ is measured normal to the body surface coinciding with $\tilde{y} = 0$.

The solution of the problem for ψ_0 posed by (7) may be written as

$$\psi_0 = \psi_{0p}(\mathbf{x}) \sum_{n=1}^{\infty} \alpha_n \cos(nt + \beta_n), \tag{8}$$

where $\psi_{0p}(\mathbf{x})$ represents the stream function for steady, irrotational flow past a cylinder with uniform flow at infinity aligned with the axis of oscillation $y = 0$.

Expanding this solution for ψ_0 close to the cylinder surface $\tilde{y} = 0$ shows that

$$\psi_0 \sim \tilde{y} V(\tilde{x}) \sum_{n=1}^{\infty} \alpha_n \cos(nt + \beta_n), \tag{9}$$

where $V(\tilde{x})$ is the surface speed for inviscid flow past the body. Since the no-slip condition is violated by (9) there must be an inner boundary layer, the Stokes layer of dimensionless thickness $O(\epsilon/R_s^{\frac{1}{2}})$ within which the viscous terms in (3), hitherto neglected, become important. Accordingly we define inner boundary-layer variables as

$$\Psi = \frac{R_s^{\frac{1}{2}}}{\epsilon} \frac{\psi}{\sqrt{2}}, \quad \zeta = \frac{R_s^{\frac{1}{2}}}{\epsilon} \frac{\tilde{y}}{\sqrt{2}}, \tag{10}$$

and seek a series solution, complementary to (5), as

$$\Psi = \Psi_0(\tilde{x}, \zeta, t, R_s) + \epsilon\{\Psi_1^{(u)}(\tilde{x}, \zeta, t, R_s) + \Psi_1^{(s)}(\tilde{x}, \zeta, R_s)\} + O(\epsilon^2), \tag{11}$$

where the steady streaming $O(\epsilon)$ has been anticipated. The leading term in (11) must match with the first-order solution (8). Guided by the inner expansion of (8), derived from (9) and (10), we write Ψ_0 as

$$\left.\begin{aligned} \Psi_0 &= V(\tilde{x}) \sum_{n=1}^{\infty} \frac{\alpha_n}{n^{\frac{1}{2}}} \mathrm{X}_{0,n}(\zeta_n)\, e^{i(nt+\beta_n)}, \\ \text{where} \qquad \zeta_n &= n^{\frac{1}{2}}\zeta. \end{aligned}\right\} \tag{12}$$

The solution for $\mathrm{X}_{0,n}$, which matches with the outer solution and satisfies the conditions on $\zeta = 0$, is the well-known Stokes solution

$$\mathrm{X}_{0,n} = \{\zeta_n - \tfrac{1}{2}(1-i)[1 - e^{-(1+i)\zeta_n}]\}. \tag{13}$$

As stated in § 1, our prime aim is to study the steady streaming represented by $\psi_1^{(s)}$ and $\Psi_1^{(s)}$. Let us return now to the outer solution of $O(\epsilon)$. Since $\nabla^2\psi_0 \equiv 0$ we have, from (3), (5) and (6),

$$\frac{\partial}{\partial t}(\nabla^2\psi_1) = \frac{\partial}{\partial t}(\nabla^2\psi_1^{(u)}) = 0,$$

from which we infer that

$$\nabla^2\psi_1^{(u)} \equiv 0. \tag{14}$$

Equation (14) yields no information about $\psi_1^{(s)}$ and therefore does not concern us directly. We do not consider $\psi_1^{(u)}$ further except to note that, exactly as in the case of purely sinusoidal oscillations, we may expect contributions to $\psi_1^{(u)}$ which are required to match with the inner solution (12), corresponding to a displacement effect, and the inner solution of $O(\epsilon)$, $\Psi_1^{(u)}$. Before returning to the steady part of the inner solution of $O(\epsilon)$, represented by $\Psi_1^{(s)}$, we consider for future reference the nature of the solution of $O(\epsilon^2)$ in the outer region. Substituting (5) into equation (3) and equating the coefficient of the terms $O(\epsilon^2)$ to zero gives

$$\frac{\partial}{\partial t}(\nabla^2\psi_2) = \frac{\partial(\psi_0, \nabla^2\psi_1^{(s)})}{\partial(x, y)},$$

from which we infer, using (8), that

$$\nabla^2\psi_2 = \phi_2(\mathbf{x}) + \sum_{n=1}^{\infty} \chi_{2,n}(\mathbf{x}) \sin(nt + \beta_n). \tag{15}$$

We are now in a position to discuss in detail the steady streaming of $O(\epsilon)$. Consider first the inner streaming represented by $\Psi_1^{(s)}$. From (3), (10) and (11) we see that the equation satisfied by $\Psi_1^{(s)}$ is

$$\frac{\partial^4 \Psi_1^{(s)}}{\partial \zeta^4} = 2\left[\frac{\partial \Psi_0}{\partial \zeta}\frac{\partial^3 \Psi_0}{\partial \tilde{x}\,\partial \zeta^2} - \frac{\partial \Psi_0}{\partial \tilde{x}}\frac{\partial^3 \Psi_0}{\partial \zeta^3}\right]^{(s)}, \tag{16}$$

where the superscript (s) on the right-hand side indicates the mean or steady part of that quantity. The terms on the right-hand side of (16) in fact represent the Reynolds stresses acting in the Stokes layer and must be evaluated using (12) and (13). It is clear that the only time-independent parts on the right-hand side of (16) can arise from interactions between terms of the same order in (12), that is from terms which involve $\cos^2(nt+\beta_n)$ or $\sin^2(nt+\beta_n)$. Consequently, just as Ψ_0 is constructed by superposing solutions from the theory involving only a single component of (1), we can similarly construct a solution for the induced streaming by writing

$$\Psi_1^{(s)} = V\frac{dV}{d\tilde{x}}\sum_{n=1}^{\infty}\frac{\alpha_n^2}{n^{\frac{3}{2}}}X_{1,n}^{(s)}(\zeta_n). \tag{17}$$

The solution for $X_{1,n}^{(s)}(\zeta_n)$ which enables us to satisfy the boundary conditions $\Psi_1^{(s)} = \partial\Psi_1^{(s)}/\partial\zeta = 0$ on $\zeta = 0$ is given by

$$X_{1,n}^{(s)} = \tfrac{13}{8} - \tfrac{3}{4}\zeta_n - \tfrac{1}{8}e^{-2\zeta_n} - \tfrac{3}{2}e^{-\zeta_n}\cos\zeta_n - e^{-\zeta_n}\sin\zeta_n - \tfrac{1}{2}\zeta_n e^{-\zeta_n}\sin\zeta_n. \tag{18}$$

The outer expansion of (17), expressed in terms of the outer variables, provides via the matching criterion a boundary condition on $\tilde{y} = 0$ for the outer streaming represented by $\psi_1^{(s)}$. This is most conveniently expressed as a 'slip-velocity' condition, say u_s, which the outer solution must satisfy. Thus

$$u_s = \epsilon\left(\frac{\partial\psi_1^{(s)}}{\partial\tilde{y}}\right)_{\tilde{y}=0} = \epsilon\left(\frac{\partial\Psi_1^{(s)}}{\partial\zeta}\right)_{\zeta=\infty} = \epsilon V\frac{dV}{d\tilde{x}}\sum_{n=1}^{\infty}\frac{\alpha_n^2}{n}\left(\frac{dX_{1,n}^{(s)}}{d\zeta_n}\right)_{\zeta_n=\infty}, \tag{19}$$

from which we deduce, using (18), that

$$\partial\psi_1^{(s)}/\partial\tilde{y} = -\tfrac{3}{4}\bar{\alpha}V\,dV/d\tilde{x} \quad \text{on} \quad \tilde{y} = 0, \tag{20}$$

where

$$\bar{\alpha} = \sum_{n=1}^{\infty}(\alpha_n^2/n). \tag{20a}$$

For a cylinder which performs simple harmonic oscillation $\alpha_1 = 1$, $\alpha_n = 0$, $n > 1$, and (20) reduces to the well-known result which may be found, for example, in Stuart (1963).

At this stage, although we have considered terms up to and including $O(\epsilon^2)$ in the outer solution, we have no further knowledge of $\psi_1^{(s)}$. To derive the equation satisfied by $\psi_1^{(s)}$ we follow the procedure adopted by Riley (1967) and consider the terms of $O(\epsilon^3)$ in (3), using (5). Since we know already that $\nabla^2\psi_0 = \nabla^2\psi_1^{(h)} \equiv 0$, we have

$$\frac{\partial}{\partial t}(\nabla^2\psi_3) - \frac{\partial(\psi_0, \nabla^2\psi_2)}{\partial(x,y)} - \frac{\partial(\psi_1, \nabla^2\psi_1^{(s)})}{\partial(x,y)} = \frac{1}{R_s}\nabla^4\psi_1^{(s)}, \tag{21}$$

and the steady part of (21) yields an equation for $\psi_1^{(s)}$. The first term on the left-hand side of (21) will only contain a steady part if ψ_3 contains a term $\propto t$. The possible meaning, and consequent rejection of such a term, has been discussed

by Riley (1967). The mean part of the second term on the left-hand side of (21) is a contribution due to the action of Reynolds stresses in the outer region. However from (8) and (15) it is readily seen that this term makes no contribution to the time-independent part of (21). Consequently the outer steady streaming is driven indirectly, by the Reynolds stresses acting in the Stokes layer, via the slip velocity given by (20). The remaining terms in (21) are easily handled so that finally, for the outer region, we see that $\psi_1^{(s)}$ satisfies the full Navier–Stokes equations with R_s as Reynolds number. Thus

$$\frac{\partial(\psi_1^{(s)}, \nabla^2\psi_1^{(s)})}{\partial(x, y)} + \frac{1}{R_s}\nabla^4\psi_1^{(s)} = 0, \tag{22}$$

with

$$\nabla\psi_1^{(s)} = o(1) \quad \text{as} \quad |\mathbf{x}| \to \infty, \tag{22a}$$

$$\left.\begin{aligned} \psi_1^{(s)} &= 0, \\ \partial\psi_1^{(s)}/\partial\tilde{y} &= -\tfrac{3}{4}\bar{\alpha}V\,dV/d\tilde{x}, \end{aligned}\right\} \quad \text{on} \quad \tilde{y} = 0. \tag{22b}$$

Apart from the constant factor $\bar{\alpha}$, defined in (20*a*), the outer streaming is determined as for the case where the vibrations of the cylinder are purely sinusoidal. Both of the conditions on $\psi_1^{(s)}$ at $\tilde{y} = 0$ arise from the matching requirement.

We are primarily interested in those cases for which $R_s \gg 1$. In such situations the outer streaming itself assumes a boundary-layer character with the thickness of the outer boundary layer of $O(R_s^{-\frac{1}{2}})$, or $O(\epsilon^{-1})$ times thicker than the Stokes layer. The work of Riley (1965) and Stuart (1966) indicates that these boundary layers develop from the two stagnation points of attachment, at which $dV/d\tilde{x} = 0$, and continue to develop, leading to an inevitable collision, which results in a thin jet emerging along the axis of oscillation. This has been demonstrated qualitatively for a circular cylinder by Schlichting (1932).

To describe the boundary-layer flow for $R_s \gg 1$ we choose as origin of coordinates on the boundary a stagnation point of attachment $\tilde{x} = \tilde{x}_s$, where $(dV/d\tilde{x})_{\tilde{x}_s} = 0$. We thus write

$$\left.\begin{aligned} \xi &= \tilde{x} - \tilde{x}_s, \\ \eta &= (\bar{\alpha}R_s)^{\frac{1}{2}}\tilde{y}, \\ \overline{\psi}_1^{(s)} &= (R_s/\bar{\alpha})^{\frac{1}{2}}\psi_1^{(s)}, \end{aligned}\right\} \tag{23}$$

and substitute into (22). Ignoring terms of relative order $R_s^{-\frac{1}{2}}$ and performing one integration with respect to η, we have, finally, for the outer boundary layer

$$\frac{\partial\overline{\psi}_1^{(s)}}{\partial\eta}\frac{\partial^2\overline{\psi}_1^{(s)}}{\partial\xi\,\partial\eta} - \frac{\partial\overline{\psi}_1^{(s)}}{\partial\xi}\frac{\partial^2\overline{\psi}_1^{(s)}}{\partial\eta^2} = \frac{\partial^3\overline{\psi}_1^{(s)}}{\partial\eta^3}, \tag{24}$$

together with

$$\left.\begin{aligned} \partial\overline{\psi}_1^{(s)}/\partial\eta &\to 0 \quad \text{as} \quad \eta \to \infty, \\ \overline{\psi}_1^{(s)} &= 0 \quad \text{on} \quad \eta = 0, \\ \partial\overline{\psi}_1^{(s)}/\partial\eta = V_s &= -\tfrac{3}{4}V\,dV/d\xi \quad \text{on} \quad \eta = 0, \\ \partial\overline{\psi}_1^{(s)}/\partial\eta &= 0 \quad \text{on} \quad \xi = 0. \end{aligned}\right\} \tag{25}$$

A novel feature of equations (24) and (25) is that, by virtue of the transformation (23), they are independent of the parameter $\bar{\alpha}$. Consequently, for these high streaming Reynolds number situations, the outer flow characteristics for any periodic motion (1) of the cylinder may be inferred directly from those for a cylinder performing simple harmonic motion.

The equation (24) together with boundary conditions (25) has been studied independently by Riley (1965) and Stuart (1966). Each author, using a different method, finally presents results for symmetric cylinders in the form of series about $\xi = 0$. Naturally, since only a few terms are calculated in each case, these series are of limited value, particularly if one wishes to extend the investigation from $\xi = 0$ up to the axis of oscillation where the boundary layers collide. Consequently, a numerical finite-difference technique has been devised for solving (24) and (25). The technique is fully implicit and is standard for two-dimensional boundary-layer calculations. The nonlinearity in (24) is handled by quasi-linearization so that at each step in the ξ direction the nonlinear algebraic equations resulting from discretization in the η direction are solved iteratively. When the difference between successive iterates falls below some prescribed tolerance the solution advances one further step in the ξ direction. In this way it is possible to 'march' from $\xi = 0$ to the axis of oscillation. Full details of this method are given by Davidson (1971), who also describes a momentum integral method which, for cylinders which are not too 'eccentric', yields reliable results very quickly. In the next section we discuss the results obtained from the theory developed here for $R_s \gg 1$, to which the finite-difference technique has been applied for a class of elliptic cylinders.

3. Application to elliptic cylinders

In order to solve (24) and (25) for a particular cylinder it is first necessary to calculate the slip velocity $V(\tilde{x})$ at the cylinder surface in steady potential flow. From this one can calculate the velocity V_s which features as a boundary condition on $\eta = 0$ in (25). We now carry out this analysis for an elliptic cylinder of semi-major and semi-minor axes a and b respectively.

Consider such a cylinder in a uniform stream U_∞ inclined at angle α to the major axis as in figure 1. To calculate the complex potential for the flow past this cylinder we first transform the $z = (x+iy)$ plane to the z^* plane, where

$$z = z^* + \lambda^2/z^*. \tag{26}$$

Here $\lambda^2 = \frac{1}{4}(a^2-b^2)$ and the radius of the circle to which the ellipse transforms is $p = \frac{1}{2}(a+b)$. The complex potential w may now be written as

$$w = U_\infty(z^* e^{-i\alpha} + p^2 e^{i\alpha}/z^*). \tag{27}$$

On the surface of the cylinder in the z^* plane we have $z^* = p e^{i\phi}$, $0 \leqslant \phi \leqslant 2\pi$ and consequently the inviscid slip velocity on the surface of the elliptic cylinder in the z plane is given by

$$U_\infty V(\phi) = \left|\frac{dw}{dz}\right| = \frac{U_\infty(1+k)\sin(\phi-\alpha)}{(\sin^2\phi + k^2\cos^2\phi)^{\frac{1}{2}}}, \tag{28}$$

where $k = b/a < 1$. Furthermore, it can be shown, if the maximum diameter $2a$ is chosen as the characteristic length d, that at the surface of the ellipse

$$\frac{d\xi}{d\phi} = \tfrac{1}{2}(\sin^2\phi + k^2\cos^2\phi)^{\frac{1}{2}}, \tag{29}$$

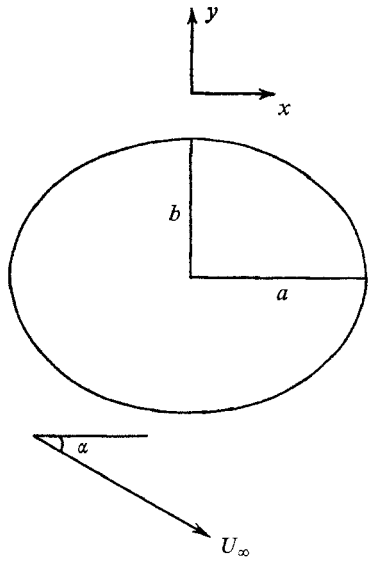

FIGURE 1. Steady flow past an ellipse.

where ξ is defined in (23). The origin of ξ is chosen to coincide with a stagnation point of the steady streaming, say $\phi = \beta$, and we define a variable $\phi_1 = \phi - \beta$. From (28) and (29) the slip velocity V_s in (25) may now be written as

$$V_s = \frac{3(1+k)^2 \sin(\phi_1+\beta-\alpha)\{(1-k^2)\cos(\phi_1+\alpha+\beta)-(1+k^2)\cos(\phi_1+\beta-\alpha)\}}{4\{\sin^2(\phi_1+\beta)+k^2\cos^2(\phi_1+\beta)\}^{\frac{5}{2}}}, \tag{30}$$

and the calculation of $V_s(\xi)$ is completed by noting that

$$\xi = \frac{1}{2}\int_0^{\phi_1} \{\sin^2(\theta+\beta)+k^2\cos^2(\theta+\beta)\}\,d\theta. \tag{31}$$

The calculation of $V_s(\xi)$ thus reduces to simple quadrature. We have carried out calculations for two special cases: (i) when the axis of oscillation coincides with the major axis of the cylinder ($\alpha = 0$, $\beta = \frac{1}{2}\pi$) and (ii) when it coincides with the minor axis ($\alpha = \frac{1}{2}\pi$, $\beta = 0$). In each case, on account of the symmetry about the major and minor axes, we need only consider the quadrant $0 \leqslant \phi_1 \leqslant \frac{1}{2}\pi$.

In figure 2 we show V_s as a function of ξ/ξ_t, where $\xi_t = (\xi)_{\phi_1=\frac{1}{2}\pi}$ is the value of ξ at the axis of oscillation, for various ellipses characterized by the parameter K. This quantity is defined as the ratio of the ellipse axis perpendicular to the axis of vibration to that parallel to the axis of vibration. Thus, when the cylinder oscillates parallel to its major axis $K = k$, and when it oscillates parallel to its minor axis $K = k^{-1}$. We note that when $k = K = 1$, the case for a circular cylinder, $V_s = 3\sin 4\xi$ and is symmetric about $\xi/\xi_t = 0{\cdot}5$. Otherwise V_s is skew-symmetric and we note, in particular, the sharp rise in V_s to a relatively high value as the axis of oscillation is approached for small values of K.

With $V_s(\xi)$ determined for these cylinders the boundary-layer equation (24) may be integrated, subject to (25), for $0 \leqslant \xi \leqslant \xi_t$ by the method described by

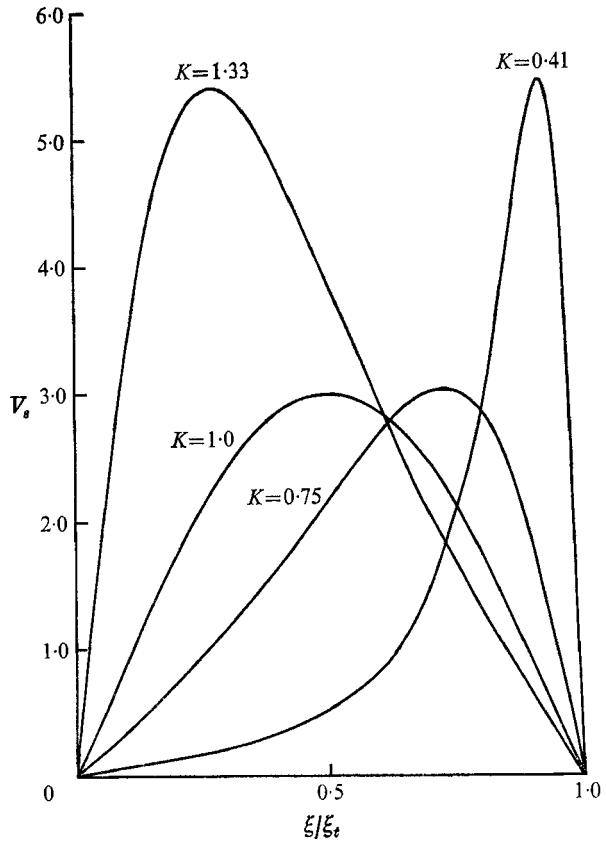

FIGURE 2. The 'slip velocity' for the outer boundary layer for various elliptic cylinders.

Davidson (1971) and outlined briefly in § 2. Velocity profiles for various values of ξ are shown in figure 3 for this outer boundary layer in the case of a circular cylinder. These show features which one may readily relate to the distribution of V_s in figure 2 for $K = 1$. We observe in addition that as $\xi \to \xi_t$ the boundary layer does not become empty, leading to the inevitable collision with the boundary layer which begins at the other attachment point. We emphasize that this notion of collision of boundary layers is only valid in the limit $R_s \to \infty$ and return to this point in the next section. The entrainment velocity v_∞ into the boundary layer is shown in figure 4 and is seen to be negative for all values of ξ. This result has been previously postulated, using a simple argument, by Riley (1965).

The jets which emerge along the axis of oscillation will have the property that the momentum flux along the jet will be invariant; this may be seen from the work of Bickley (1937). Clearly, then, the momentum flux in the outer boundary layer under discussion is an important quantity. In figure 5 we show the momentum flux

$$M(\xi/\xi_t) = \int_0^\infty \left(\frac{\partial \overline{\psi}_1^{(s)}}{\partial \eta}\right)^2 d\eta \tag{32}$$

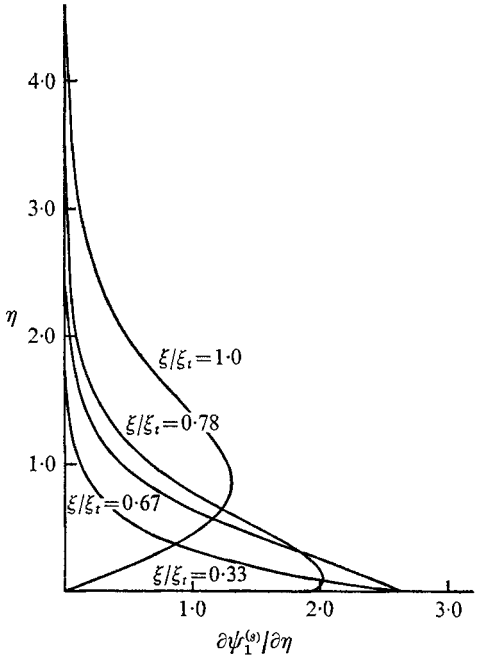

FIGURE 3. Velocity profiles, at various stations, in the outer boundary layer for a circular cylinder ($K = 1$).

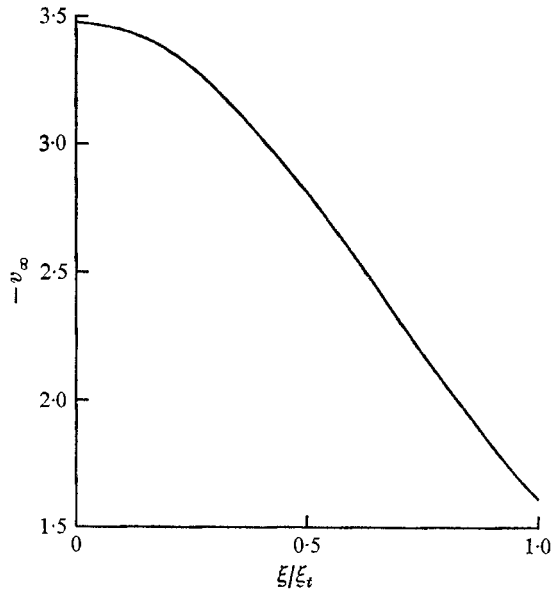

FIGURE 4. The entrainment velocity into the outer boundary layer for a circular cylinder ($K = 1$).

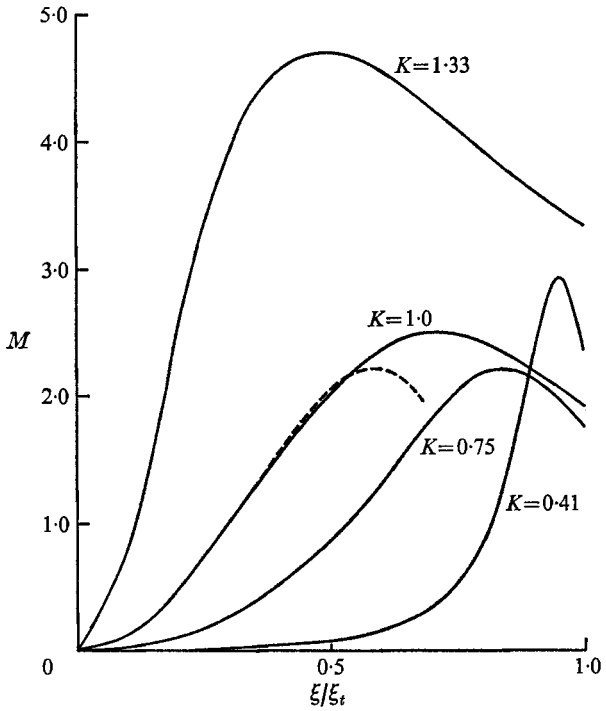

FIGURE 5. The momentum flux in the outer boundary layer for various elliptic cylinders. ———, momentum flux for $K = 1{\cdot}0$ calculated from the series solution given by Riley (1965).

in the outer boundary layer as a function of ξ/ξ_t for various values of K. In figure 6 we show the quantity $N = 2M(1)$ as a function of K, calculated from the terminal boundary-layer momentum flux. This parameter will determine the strength of the jet. We observe that N exhibits an unexpected minimum at $K \approx 0{\cdot}8$. Consideration of the distribution of $M(\xi)$, and its relation to the velocity V_s shown in figure 2, indicates that the relatively small increase in N for values of $K < 0{\cdot}8$ may be attributed to the boost given to the boundary-layer flow close to the axis of oscillation for small K. Care must be exercized in interpreting these results since, of course, no jet can be expected from the vibrations of a flat plate in its own plane, corresponding to $K \equiv 0$. In fact the theory developed above will only be valid for $kR_s^{\frac{1}{2}} \gg 1$ if the boundary layer is to remain thin compared with the thickness of the ellipse, as we have implicitly assumed.

The relatively simple physical situation which we have studied in §§ 2 and 3, together with the unexpected result shown in figure 6, has prompted a rudimentary experimental investigation which we now describe.

4. Experiments

In the experimental programme only limited facilities were available, and our primary aim has been to measure the strength of the jet along the axis of oscillation which results from the collision of the boundary layers. This has been

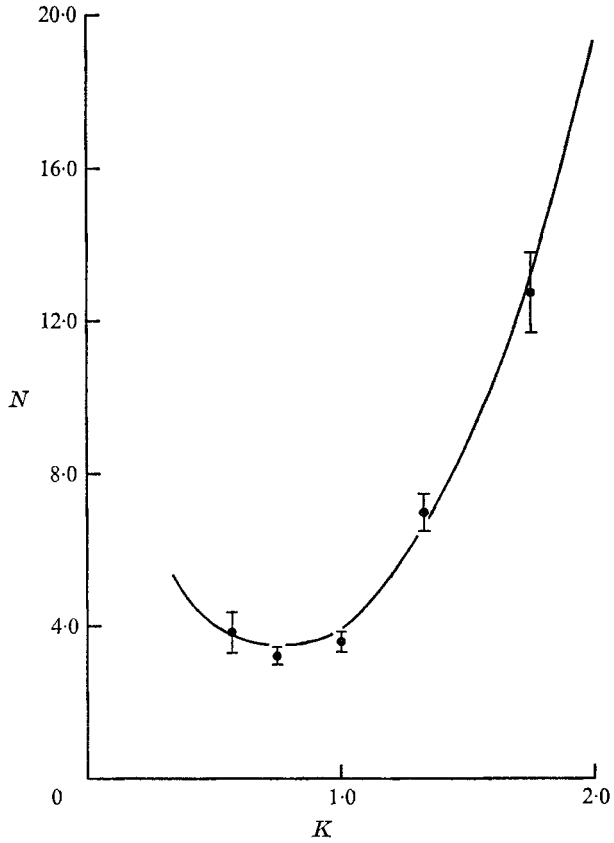

FIGURE 6. The contribution to the terminal momentum flux from both boundary layers as a function of K. ●, mean for the experimental results included here. The error bars represent the standard deviation of the mean. The numbers of readings used for each cylinder are as follows: 9 for $K = 0{\cdot}57$, 6 for $K = 0{\cdot}75$, 7 for $K = 1{\cdot}0$, 10 for $K = 1{\cdot}33$ and 4 for $K = 1{\cdot}75$.

accomplished by a simple flow visualization technique shown schematically in figure 7. The vibrating cylinder was submerged in a tank of water and oscillated vertically. Across the jet a thin wire was placed, and through this wire a pulsating current was passed to release lines of hydrogen bubbles. These lines of bubbles rise from the wire and are distorted to show the jet structure quite clearly. Quantitative measurements are made from photographic records.

In the theory described in §§ 2 and 3 the outer boundary-layer calculations were continued up to the axis of oscillation $\xi = \xi_t$. Of course, the boundary-layer equations break down before that point is reached, in fact within a distance of $O(R_s^{-\frac{1}{2}})$ from ξ_t. In a region centred upon the point O of the cylinder in figure 7, which coincides with the axis of oscillation, and of typical dimension $O(R_s^{-\frac{1}{2}})$, the flow is effectively inviscid. During an early sequence of experiments to establish qualitatively the presence of the jet, dye was injected into the boundary layer at various points around the cylinder. It is interesting to note that there was no 'trapping' of the dye in this inviscid region indicating that no closed streamlines are present. It is within this region that the flow changes direction and

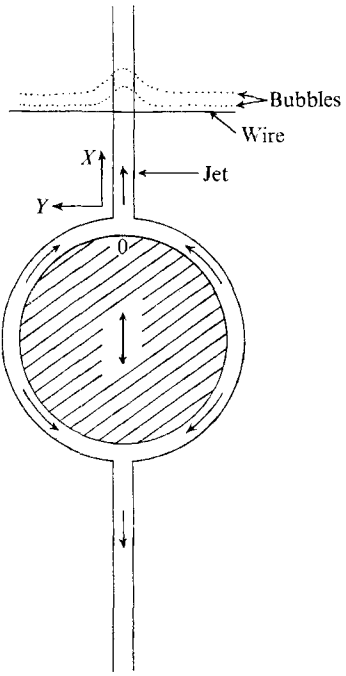

FIGURE 7. Schematic representation of the jet and flow visualization technique.

from which it emerges as the jet shown in figure 7. Similar situations have been encountered by Stewartson (1958) and Lyne (1971), in different physical contexts. Both these authors conclude that the velocity profiles at the end of each boundary layer are convected around and emerge essentially unchanged on this scale. We assume this to be the case here so that, in particular, the momentum flux in the jet is proportional to $N = 2M(1)$, where M is defined in equation (32).

The similarity solution for the two-dimensional jet given by Bickley (1937) may be described as follows. If $\tilde{\psi}_1^{(s)}$ is the dimensional stream function for the jet then with (X, Y) as dimensional co-ordinates, with origin at the mean position of O in figure 7,

$$\left.\begin{aligned} \tilde{\psi}_1^{(s)} &= (9N_1\nu(X-X_0)/2\rho)^{\frac{1}{3}}\tanh\tilde{\eta}, \\ \text{where} \qquad \tilde{\eta} &= (N_1/48\rho^2\nu^2(X-X_0)^2)^{\frac{1}{3}}\,Y, \end{aligned}\right\} \tag{33}$$

so that the dimensional axial velocity $\tilde{u}_s$ along the jet is given by

$$\tilde{u}_s = (3N_1^2/32\rho^2\nu(X-X_0))^{\frac{1}{3}}\operatorname{sech}^2\tilde{\eta}. \tag{34}$$

In equations (33) and (34)

$$N_1 = \int_{-\infty}^{\infty} \rho\tilde{u}_s^2\,dY$$

is the momentum flux per unit depth in the jet, and X_0 is an arbitrary constant which simply reflects the uncertainty of the location of the origin for the similarity solution. From the manner in which our jet is formed it is clear that the initial velocity profile will not correspond to (34). However, our experimental results

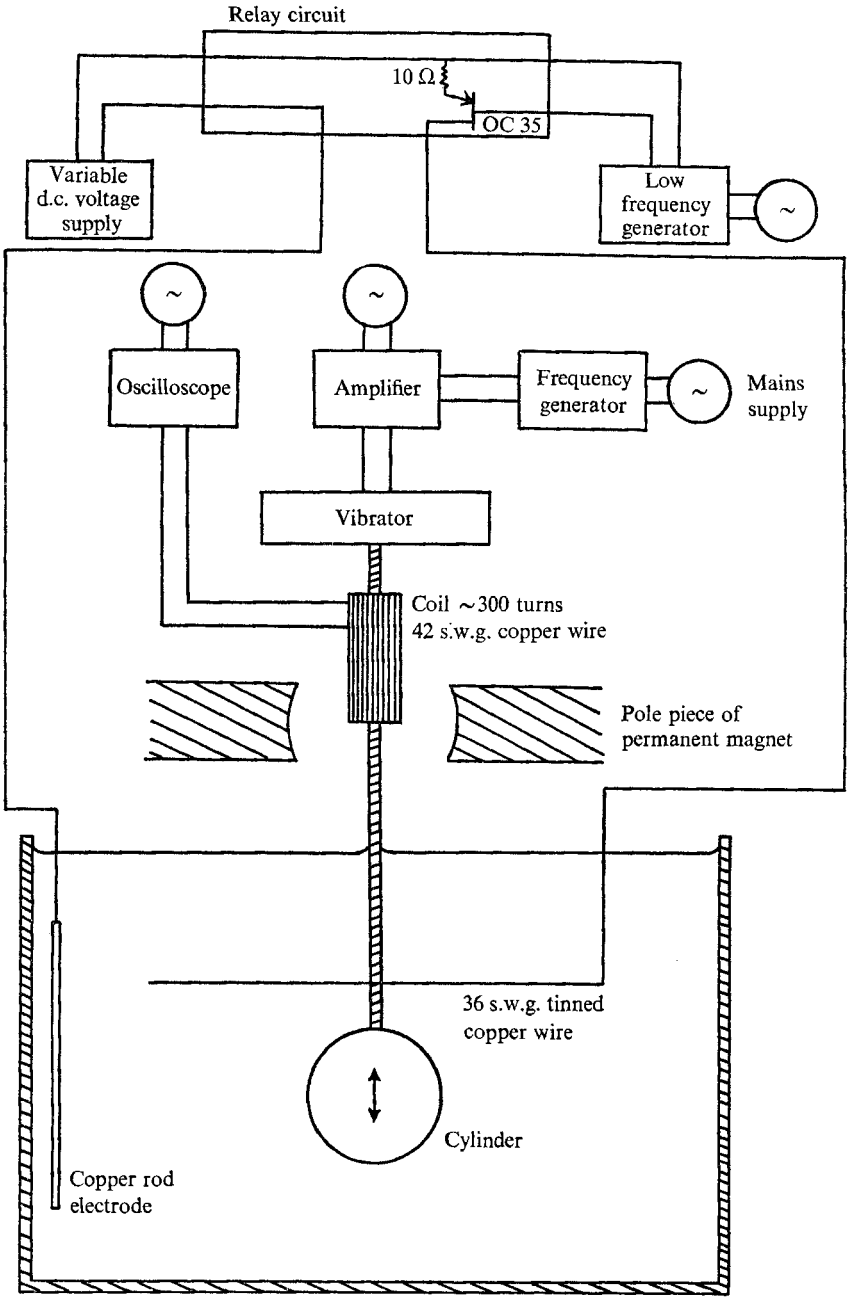

FIGURE 8. Schematic representation of the experiment.

indicate that the similar profiles are achieved within about one diameter from the point at which the jet emerges. We now describe our experimental procedure in greater detail.

The experimental set-up is shown schematically in figure 8. The cylinders, typically 30 cm in length and 2 cm in diameter, were submerged in water to

which a small quantity of salt ($\approx 0{\cdot}1$ g/l) was added in a tank of cross-section 28×26 cm and length 58 cm. The vertical oscillations of the cylinder were induced mechanically by a vibrator which was activated electromagnetically. The amplitude and frequency of the vibrations could be varied over a fairly wide range. On the brass shaft connecting the cylinder and vibrator we incorporated a coil of approximately 300 turns of 42 s.w.g. copper wire. This was placed between the pole pieces of a permanent magnet and the induced e.m.f. in this coil, which is proportional to the velocity, was monitored on an oscilloscope. A typical trace is shown in figure 9(*a*) (plate 1). In this way, from our knowledge of the amplitude of the oscillation, which was measured using a travelling microscope, we were able to calculate the velocity of the vibrating cylinder. In all cases the motion of the cylinder was a distorted simple harmonic motion to which we can apply the theory of § 2. As we have already mentioned, the flow was visualized by releasing hydrogen bubbles into the fluid over the cylinder. This was achieved by stretching a length of 2 amp tinned copper fuse wire horizontally over the cylinder and perpendicular to its generators. A potential difference was applied between this wire and a copper rod electrode immersed in the liquid. The voltage provided was obtained from a variable d.c. source and the supply was pulsed using a simple relay circuit, shown in detail in figure 8, in connexion with a low frequency generator. The frequency of the pulse and the applied potential difference were varied until a well-defined succession of velocity profiles was observed. Strong side lighting along the wire showed, by scattered light, the hydrogen bubbles very clearly against a dark background. These were photographed on Ilford FP 4 film using an exposure of $\frac{1}{60}$ s.

In the experiments lines of hydrogen bubbles were released at fixed, predetermined intervals from the wire. These lines rise freely but are distorted by any fluid motion which exists and the jet structure can be clearly visualized, as for example in figure 9(*b*) (plate 1). From such photographs quantitative measurements may be made. The relationship between the measured momentum flux N_1 in the jet and the parameter N of figure 6 can be shown to be

$$\frac{N_1}{\rho d U_\infty^2}\left(\frac{R_s^{\frac{1}{2}}}{\epsilon^2 \overline{\alpha}^{\frac{3}{2}}}\right) = N. \tag{35}$$

Quite apart from the fact that it was not easy to create an approximately two-dimensional symmetric flow, experimental difficulties associated with the flow visualization technique were encountered. Too large a current passing through the wire created an apparently continuous stream of large bubbles from the wire. Even for moderately large currents the striations in the fluid represented by the lines of bubbles become distorted by an instability caused by the local aggregation of bubbles. In the experiments currents ≈ 30 ma at ≈ 15 V d.c. were used, but even then the formation of a relatively large stationary bubble at the wire was always a potential hazard. The current was pulsed through the wire at frequencies in the range 3–6 c/s. The optimum position of the wire relative to the cylinder, and the amplitude and frequency of the cylinder vibration were found by trial and error. Typically, with the wire about one diameter from the cylinder, and with an amplitude and frequency 0·1 cm and 45 c/s respectively,

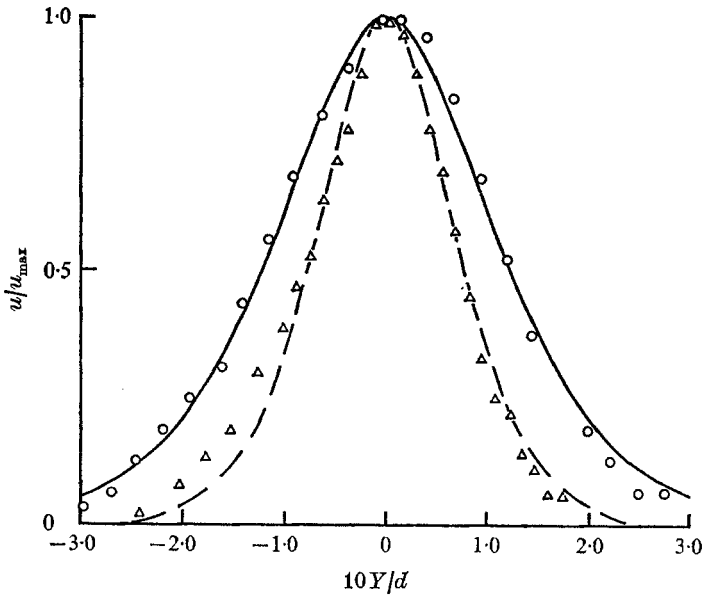

FIGURE 10. A comparison between the theoretical jet solution due to Bickley (1937) and typical experimental profiles over a circular cylinder. For $N_1 = 0{\cdot}35$ g/s^2: ———, theory; ○, experiment. For $N_1 = 0{\cdot}61$ g/s^2: – – –, theory; △, experiment.

the best results were obtained, with measured velocities in the fluid of the order 1 cm/s. Thus in the experiments $\epsilon \approx 0{\cdot}05$, $R_s \approx 300$. The experiments were carried out using five cylinders corresponding to $K = 0{\cdot}57$, 0·75, 1·00, 1·33 and 1·75. The elliptic cylinders were fashioned from balsa wood and suitably sealed. The results from the measured momentum flux are compared, using (35), with the theoretical prediction in figure 6. Correlation of experimental results with the theory involves U_∞^3, as may be seen from (35). Thus any error in the measurement of the amplitude of the vibration is raised to the third power. This measurement, along with the interpretation of the photographic records, proved to be the weakest point in our experimental investigation and is up to 5 % in error. For each cylinder a large number of photographs of the jet profiles were analysed and the results from this analysis are shown in figure 6. Greater difficulty was experienced in obtaining results for the slender ellipses although the relatively strong, very thin jet predicted theoretically was clearly visible to the eye. In figure 10 a comparison is made between the theoretical velocity profile (34) and two profiles which are representative of those obtained experimentally using the circular cylinder. The parameter X_0 was chosen by matching the maximum velocity predicted by (34) with the experimental maximum. From the comparison in figure 10 it appears that the flow in the jet assumes its similarity form very quickly. With the wire in a lower position, particularly for the smaller values of K, the doubly peaked profile from which the jet is initially formed has been observed.

Some of the limitations of the technique we have employed in our experimental investigation have been mentioned. Others include three-dimensional and finite amplitude effects. For the latter we note that $\epsilon R_s^{\frac{1}{2}}$, which is assumed small in the

theory, was approximately 0·8 in the experiments. However within all these limitations (we remark that none of our equipment was purpose-built), we are encouraged by the consistency between the theoretical and experimental results.

We are indebted to our physics colleagues for the loan of expensive pieces of apparatus which would, otherwise, have been completely unavailable. One of us (B.J.D.) was in receipt of an S.R.C. studentship during the period in which this work was carried out.

REFERENCES

Bickley, W. G. 1937 *Phil. Mag.* **23**, 727.
Davidson, B. J. 1971 Ph.D. thesis, University of East Anglia.
Longuet-Higgins, M. S. 1953 *Phil. Trans.* A **245**, 535.
Lyne, W. H. 1971 *J. Fluid Mech.* **45**, 13.
Riley, N. 1965 *Mathematika*, **12**, 161.
Riley, N. 1967 *J. Inst. Math. Applics.* **3**, 419.
Schlichting, H. 1932 *Phys. Z.* **33**, 327.
Stewartson, K. 1958 *Proc. Symp. b.l. Res. Freiburg i Br.* 1957, pp. 57–91. Springer.
Stuart, J. T. 1963 *Laminar Boundary Layers*, chap. 7. Oxford University Press.
Stuart, J. T. 1966 *J. Fluid Mech.* **24**, 673.

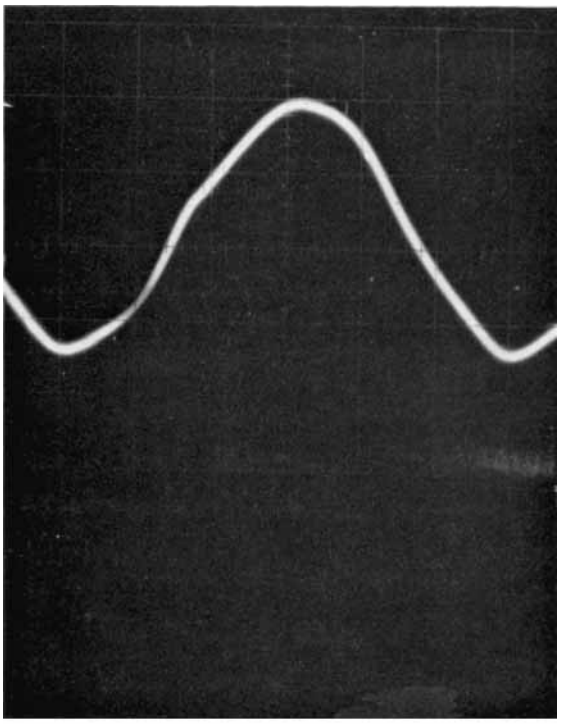

(*a*)

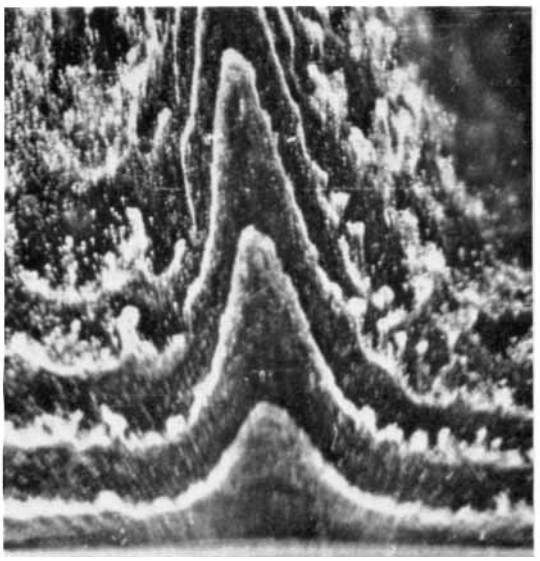

(*b*)

FIGURE 9. Photographs of (*a*) a typical oscilloscope trace of the cylinder velocity, (*b*) an enlargement (× 4) of the visualized flow structure in the jet over a circular cylinder.